MALAYSIAN JOURNAL OF ANALYTICAL SCIENCES

Journal homepage: https://mjas.analis.com.my/

Research Article

Degradation of methyl orange by Fe(III) TAML/H_2O_2 catalytic system: Response surface analysis of process parameters

Siti Nur Khairunnisa Mahassan, Nabilah Ismail*, and Nora Salina Md Salim

Faculty of Science and Marine Environment, Universiti Malaysia Terengganu, 21030 Kuala Nerus, Terengganu, Malaysia

*Corresponding author: nabilah.i@umt.edu.my

Received: 23 September 2025; Revised: 16 January 2026; Accepted: 23 February 2026; Published: 30 April 2026

Abstract

Methyl Orange (MO) is a synthetic azo dye widely used in textile and laboratory applications and is classified as a micropollutant due to its toxicity, persistence, and resistance to conventional wastewater treatment processes. In this study, the catalytic degradation of MO was investigated using a homogeneous Fe(III)-TAML/H_2O_2 system, with emphasis on evaluating the effects and interactions of key process parameters using Response Surface Methodology (RSM). A Central Composite Design (CCD) was employed to evaluate the effects and interactions of four independent variables, namely pH, stirring speed, catalyst ratio, and dye ratio, on the percentage degradation of MO. The developed quadratic model exhibited strong statistical significance ($R^2 = 0.9178$) and revealed significant interaction and non-linear effects among the operating parameters. Based on the model-predicted conditions, high MO degradation (96.43%) was observed at pH 9.5, stirring speed 500 rpm, catalyst ratio 1, and dye ratio 100. Experimental validation under these conditions achieved 92.33% degradation, with a deviation of less than 5% from the predicted value, confirming the model's reliability. Across the experimental domain, MO degradation efficiencies ranged from approximately 5% to over 94%, depending on operating conditions. The results demonstrated that the Fe(III)-TAML/H_2O_2 catalytic system was a highly efficient and environmentally sustainable advanced oxidation process (AOP) for the removal of azo dyes. The conditions identified in this study provided valuable quantitative guidance for the application of this catalytic system in practical wastewater treatment, particularly for dye-contaminated effluents.

Keywords: response surface methodology, degradation, methyl orange, catalytic system

Introduction

Water pollution has emerged as one of the most pressing environmental challenges worldwide, driven by rapid industrialization, population growth, and increasing demand for water resources. It is estimated that more than 80 % of the world's wastewater is discharged into the environment without adequate treatment, resulting in severe degradation of ecosystems and contamination of surface and groundwater resources [1]. The discharge of complex and hazardous industrial effluents poses significant risks to environmental sustainability and public health, particularly in regions with limited wastewater treatment infrastructure.

Within the broad spectrum of industrial wastewater contaminants, synthetic dyes represent a particularly critical class of pollutants due to their widespread use, high visibility in aquatic environments, and strong resistance to degradation. As a result, dye-containing effluents have become a major focus of wastewater treatment research, especially in efforts aimed at mitigating persistent water pollution. Among industrial sources, the dye industry is a major contributor to water pollution, owing to the extensive use of synthetic dyes in textile, paper, cosmetic, pharmaceutical, and laboratory applications [2].

Furthermore, the scale of this problem is substantial: global dye production exceeds 700, 000 tons annually, and approximately 10-15% of the dye used in industrial processes are lost during dyeing operations and released directly into wastewater

streams [3]. Even at low concentrations, dyes impart intense colouration to water bodies, reducing light penetration, inhibiting photosynthesis, and disrupting aquatic ecosystems. Synthetic dyes are deliberately designed to be chemically stable and resistant to fading, properties that enhance their performance in industrial applications but make them particularly difficult to remove during wastewater treatment. Since the discovery of the first synthetic dye in 1856, dye production has increased exponentially, with azo dyes accounting for approximately 60-70% of all commercially produced dyes due to their high colour intensity, structural stability, and low production cost [4]. These characteristics render azo dyes persistent in aquatic environments and resistant to degradation by conventional treatment processes.

Additionally, Methyl Orange (MO), a widely used anionic azo dye, contains sulfonate ($-SO_3^-$) groups and one or more azo (–N=N–) linkages that connect aromatic rings, which confer high chemical stability and resistance to biodegradation [5,6]. As a result, MO persists in aquatic environments and poses significant ecological and health risks, including toxicity to aquatic organisms and potential mutagenic and carcinogenic effects in humans [7,8]. Even at low concentrations, MO imparts strong colouration to water bodies, reducing light penetration and disrupting photosynthetic activity, thereby affecting aquatic ecosystems.

Despite extensive research, conventional wastewater treatment technologies remain inadequate for the complete removal of azo dyes. Physical methods such as adsorption merely transfer dyes from the aqueous phase to solid media, generating secondary waste that requires further treatment [6,9]. Chemical coagulation and flocculation processes produce large volumes of sludge, increasing disposal costs and environmental burden [5,9]. Biological treatment methods are often ineffective due to the complex aromatic structures and strong azo linkages that resist microbial degradation, frequently resulting in incomplete mineralization and the formation of potentially more toxic intermediates [6,7,9]. These limitations highlight the need for more efficient and sustainable treatment strategies that degrade refractory dye molecules rather than simply remove them.

In this context, advanced oxidation processes (AOPs) have emerged as promising alternatives for treating dye- laden wastewater because they generate highly reactive oxygen species (ROS), such as hydroxyl radicals (•OH) and superoxide anions ($O_2^{\bullet-}$), which can non-selectively oxidize and mineralize persistent organic pollutants into harmless end products such as CO_2 and H_2O [5,10]. Among various AOPs, hydrogen peroxide–based catalytic systems have gained considerable attention due to their environmental compatibility and strong oxidative capacity upon activation by suitable catalysts [11,12]. The Fe(III)-tetra-amido macrocyclic ligand (Fe(III)TAML) catalyst represents a new generation of biomimetic catalysts that activate H_2O_2 under mild conditions to form high-valent iron–oxo species capable of oxidizing a wide range of organic contaminants [13-15]. Compared with traditional Fenton systems, Fe(III)TAML/H_2O_2 offers several advantages, including operation over a broader pH range, high catalytic stability, minimal iron sludge formation, and lower toxicity [12,14].

Beyond intrinsic catalytic activity, the effectiveness of the Fe(III)TAML/H_2O_2 system depends strongly on the chemical compatibility and interactions among its components, including the dye molecule, catalyst, oxidant, and solution environment. MO exists predominantly as a negatively charged species under neutral to alkaline conditions due to its sulfonate groups, while the Fe(III)TAML catalyst operates as a homogenous complex capable of activating hydrogen peroxide in solution. In such a system, degradation proceeds primarily through solution-phase reactions involving ROS and high-valent iron–oxo intermediates rather than surface adsorption. Hydrogen peroxide serves as a green and compatible oxidant, efficiently activated by the Fe(III)TAML without excessive non-productive decomposition when appropriate operating conditions are maintained. Additionally, solution pH influences dye ionization, catalyst stability, and oxidant behaviour, while catalyst and dye ratios govern the balance between reactive species generation and target pollutant availability. The interplay among these factors ultimately controls degradation efficiency and process sustainability.

However, several critical issues in Fe(III)TAML/H_2O_2 systems remain unresolved. Previous studies have primarily focused on reaction mechanisms, catalyst design, and pollutant degradation pathways, while systematic optimization of operational parameters has received limited attention. In particular, the influence of catalyst-to-dye ratio and solution pH, as well as their interaction with the dye-to-dye ratio, on degradation efficiency remains poorly established. Excessive catalyst loading may lead to non-productive H_2O_2 decomposition and radical scavenging, reducing treatment efficiency, whereas insufficient catalyst dosage limits oxidant activation [13–15]. Similarly, pollutant concentration can significantly affect

apparent degradation kinetics, yet this factor is often treated independently rather than in combination with catalyst loading. Furthermore, although Fe(III)TAML catalysts are reported to operate under mild alkaline conditions, the optimal pH window for maximizing dye degradation while minimizing oxidant loss remains unclear.

These knowledge gaps indicate that systematic optimization is essential to fully exploit the catalytic potential of the Fe(III)TAML/H_2O_2 system. Without systematic optimization, the process may suffer from inefficient oxidant utilization, unnecessary chemical consumption, and reduced scalability for real wastewater applications. Therefore, the present study addresses these limitations by applying Response Surface Methodology (RSM) coupled with Central Composite Design (CCD) to systematically investigate and optimize the catalytic degradation of MO using the Fe(III)TAML/H_2O_2 system. This study simultaneously evaluates the effects of individual and interactive effects of pH, stirring speed, catalyst ratio, and dye ratio as key operational parameters. Analysis of Variance (ANOVA) was applied to evaluate the statistical significance of individual factors and their interactions [16,17]. The novelty of this work lies in establishing quantitatively optimized reaction conditions for Fe(III)TAML-catalyzed MO degradation, with particular emphasis on catalyst-to-dye ratio interactions and alkaline pH behaviour, which have not been comprehensively reported in previous studies. The findings aim to bridge existing knowledge gaps and provide practical design guidelines for the efficient and sustainable application of Fe(III)TAML/H_2O_2 systems in dye wastewater treatment.

Materials and Methods

Purification of MO

Purified MO was used in this study to ensure accurate and reproducible evaluation of the Fe(III)TAML/H_2O_2 catalytic degradation process, as impurities present in commercial dyes might interfere with ROS and UV-Vis absorbance measurements.

The MO stock solution was prepared by adding 200 mg of solid MO in a solution of methanol and deionized water (9:1) v/v (4.5 mL methanol and 0.5 mL deionized water) with stirring. This solvent system was selected to enhance the solubility of the aromatic azo dye while maintaining stabilization of its sulfonate functional groups. Any remaining insoluble material was removed via filtration.

Purification was performed using silica gel column chromatography to remove residual impurities that could affect degradation kinetics and spectrophotometric analysis. A 2 mL sample mixture was added and retained in the column, and elution was performed using a methanol/water solvent system. The progress of elution was initially monitored visually by the appearance of the characteristic, orange-coloured fraction; however, fraction collection and selection were based on quantitative UV-Vis spectroscopic analysis rather than visual observation.

MO exhibited a characteristic maximum absorption wavelength (λ_{max}) at approximately 464 nm, as reported in Bawazeer (2024) and confirmed experimentally in this study. Eluted fractions displaying identical λ_{max} values and consistent absorbance intensities at 464 nm (variation within ±5%) were considered compositionally uniform and were used for subsequent experiments.

Blank experiment

This blank experiment measured the degradation of MO in the absence of a catalyst and H_2O_2 solution. Then, MO was degraded by the Fe(III)TAML catalyst in the absence of H_2O_2, and finally, MO was degraded by O_2 in the absence of the Fe(III)TAML catalyst.

Analysis method

In this study, the concentration of MO dye was analyzed using a UV-Vis spectrophotometer (Shimadzu UV-160A, Shimadzu Corporation, Kyoto, Japan) by measuring the absorbance of untreated samples at a maximum wavelength of 464 nm. The degradation efficiency of MO dye was calculated as a percentage using the following Equation 1:

$$Degradation\ (\%) = \frac{A_0 - A_t}{A_t} x\ 100 \qquad (1)$$

where A_0 and A_t denote the initial and time-dependent absorbance, respectively.

Experimental design and response surface analysis of bleaching MO

The experiments were conducted at an equilibrium time of 1 hour to investigate the effects of four independent variables: the pH of the carbonate buffer (X_1), stirring speed (X_2), catalyst ratio (X_3), and dye ratio (X_4). The ranges of these variables were selected based on preliminary experiments, relevant literature, and practical considerations related to catalyst performance and reaction feasibility. The pH range was chosen to cover mild alkaline conditions where the Fe(III)TAML catalyst had been reported to exhibit high catalytic activity and stability. The stirring speed range was selected

to ensure sufficient mixing and mass transfer without causing excessive turbulence. The catalyst ratio and dye ratio ranges were selected to represent low, intermediate, and high catalyst-to-dye conditions (corresponding to actual ratios of 1, 50.5, and 100), allowing evaluation of insufficient oxidant activation at low ratios and potential radical scavenging or non-productive oxidant decomposition at high ratios.

Each variable was examined at three coded levels (-1, 0, and +1), as shown in **Table 1**. The design included 30 runs derived from a 2^4 full-factorial design combined with six central and eight axial points. RSM was performed using Design-Expert software (Stat-Ease Inc., USA) with a face-centered CCD. This system used a buffer solution combining dye and H_2O_2 to promote dye degradation in an Fe-TAML beaker [13,14]. The solution volume was 20 mL, consisting of carbonate buffer (18.9 mL, 0.01 M, pH 9.5), H_2O_2 (1.0 mM, 0.1 mL), Fe-TAML (1 mL, 1.0 µmole, 50µM; Mw of Fe(III)-TAML was 667.32 provided by GreenOx), and MO (50 µM, 1.0 µmole). The solution was stirred using a magnetic stirrer (MSH-20D WiseStir, Daihan Scientific, Korea). For monitoring, an aliquot (3 mL) of the solution was transferred to a quartz cuvette, and its absorbance was measured every 5 min using UV-Vis Spectroscopy (UV-1800, Shimadzu, Japan). The absorbance at the maximum wavelength (λmax = 464 nm) was used to monitor MO degradation. After each measurement, the same aliquot was returned to the beaker. The absorbance was monitored over time to track the degradation of MO. Continuous monitoring was performed to observe the progression of colour removal; however, the response variables used for all experimental runs were the percentage degradation measured after a fixed reaction time of 1 hour. The response variable was the percentage degradation of MO after a fixed reaction of 1 hour, calculated from the change in absorbance at 464 nm relative to the initial value.

Table 1. Process variables: the level of the independent variables

Independent Variables	Coded	Range and Level		
		-1	0	+1
pH	X_1	9.5	10.25	11
Stirring Speed (rpm)	X_2	200	500	800
Catalyst Ratio	X_3	1	50.5	100
Dye Ratio	X_4	1	50.5	100

The experimental data were fitted to a second-order polynomial model to evaluate the relationships between the response and the four independent variables. The general form of the model used was Equation 2:

$$Y = \beta_0 + \sum_{i=1}^{4} \beta_i X_i + \sum_{i=1}^{4} \beta_{ii} X_i^2 + \sum_{i<j}^{4} \beta_{ij} X_i X_j + \varepsilon \quad (2)$$

Where Xi and Xj represent the coded independent variables, $\beta 0$ is the intercept, βi, βii, and βij are the linear, quadratic, and interaction coefficients, respectively, and Y is the predicted response.

Results and Discussion

This section presents the findings of the study, including statistical analysis, the effect of the key process variables, response surface analysis, and model validation. The results are discussed in detail in the following subsections.

Statistical analysis of fitting models

Table 2 presents the percentage degradation of MO for different dye degradation runs. The experimental data were fitted to Equation 2 to predict dye degradation as a function of pH, stirring speed, catalyst ratio, and dye ratio.

Table 3 presents the ANOVA of the second-order polynomial model for the four independent variables on degradation efficiency. The model had an F-value of 17.79, indicating significance, and the probability of a substantial F-value arising from noise was approximately 0.01%. P-values that were less than 0.0500 indicated that the model terms were significant. The results showed that X_1 (pH), X_3 (catalyst ratio), X_4 (dye ratio), X_3X_4 (interaction between catalyst ratio and dye ratio), and X_3^2 (quadratic effect of catalyst ratio) were significant. The lack-of-fit term was not significant, indicating that the model adequately represented the experimental data.

To improve the model's accuracy and simplicity, non-significant terms were removed via backward elimination. This refinement was motivated by the noticeable difference between the predicted R^2 (0.6591) and adjusted R^2 (0.8902) values observed in the full model, as summarized in the fit statistics in **Table 3**. **Table 4** presents the ANOVA table for the reduced quadratic model, and it confirms that the refined model was significant, with improved predicted and adjusted R^2 values of 0.8661 and 0.9007, respectively. The lack-of-fit for the reduced model was not significant ($p > 0.05$), indicating good agreement between the model and the experimental data. These results demonstrated the effectiveness of the model refinement process, which retained only the significant factors affecting degradation efficiency while minimizing noise and potential bias.

Table 2. CCD experiment and experimental results

Experiment Number	Experimental Design				Experimental Plan				Observed % Y	Predicted % Y
	pH	Speed (rpm)	Catalyst ratio	Dye ratio	X_1	X_2	X_3	X_4		
1	0	0	0	0	10.25	500	50.5	50.5	22.08	32.20
2	-1	+1	-1	+1	9.5	800	1	100	90.73	98.77
3	+1	0	0	0	11	500	50.5	50.5	45.15	32.50
4	-1	-1	-1	+1	9.5	200	1	100	91.12	89.74
5	0	0	0	0	10.25	500	50.5	50.5	33.88	32.20
6	+1	-1	-1	+1	11	200	1	100	94.42	91.27
7	+1	+1	+1	+1	11	800	100	100	12.63	24.00
8	-1	+1	+1	-1	9.5	800	100	1	17.36	23.87
9	-1	-1	-1	-1	9.5	200	1	1	63.44	55.43
10	-1	0	0	0	9.5	500	50.5	50.5	33.50	41.46
11	0	0	0	+1	10.25	500	50.5	100	46.85	43.62
12	-1	-1	+1	+1	9.5	200	100	100	25.68	27.08
13	0	+1	0	0	10.25	800	50.5	50.5	48.30	38.34
14	+1	-1	+1	-1	11	200	100	1	12.56	7.88
15	0	0	0	0	10.25	500	50.5	50.5	29.31	32.20
16	0	0	-1	0	10.25	500	1	50.5	66.75	65.42
17	0	0	0	0	10.25	500	50.5	50.5	28.03	32.20
18	+1	-1	+1	+1	11	200	1	1	45.15	54.55
19	-1	+1	-1	-1	9.5	800	1	1	59.18	56.04
20	-1	-1	+1	-1	9.5	200	100	1	18.13	18.33
21	0	0	0	0	10.25	500	50.5	50.5	31.16	32.20
22	0	0	0	0	10.25	500	50.5	50.5	34.66	32.20
23	0	0	0	-1	10.25	500	50.5	1	18.13	16.67
24	0	0	+1	0	10.25	500	100	50.5	16.58	13.22
25	+1	+1	+1	-1	11	800	100	1	5.22	4.41
26	-1	+1	+1	+1	9.5	800	100	100	52.63	41.40
27	+1	-1	+1	+1	11	200	100	100	18.10	19.05
28	0	-1	0	0	10.25	200	50.5	50.5	30.29	35.56
29	+1	+1	-1	+1	11	800	1	100	93.68	91.29
30	+1	+1	-1	-1	11	800	1	1	44.18	46.15

The response equation for degradation efficiency is as follows:

$$\text{Degradation (\%)} = 33.445 - 4.4822X_1 - 26.0978X_3 + 13.4717X_4 - 6.3894X_3X_4 + 12.5294X_3^2 \quad (3)$$

Transform into actual factors

$$\text{Degradation (\%)} = 113.974 - 5.9763\ (\text{pH}) - 0.9120\ (\text{Catalyst Ratio}) + 0.4038\ (\text{Dye Ratio}) - 0.0026\ (\text{Catalyst Ratio} \times \text{Dye Ratio}) + 0.0051\ (\text{Catalyst Ratio})^2 \quad (4)$$

The equation expressed in coded factors allowed prediction of the response at specific factor settings. Typically, the high and low levels of each factor are represented as +1 and -1, respectively. This coded form was helpful for comparing the coefficients to assess each factor's relative influence, whereas the equation in actual units was used to predict responses at real factor levels [16].

The model's predicted degradation values were obtained by substituting the independent variables into the equation and comparing the resulting values with the experimental results. As shown in **Figure 1**, the data points cluster near the diagonal line, indicating strong agreement between the measured and predicted degradation. This indicates that the CCD adequately captured the relationship between the process variables and degradation efficiency, confirming the suitability of the model for response

surface and effect analysis. The accompanying **Figure 2** further supported the model's adequacy, with residuals following an approximately straight-line pattern, confirming that the error distribution was normal and the model assumptions were valid.

Table 3. ANOVA for the quadratic model of degradation efficiency

Source	Sum of Square	dF	Mean Square	F-value	p-value	
Model	18160.41	14	1297.17	17.79	< 0.0001	Significant
X_1	361.63	1	361.63	4.96	0.0417	
X_2	34.78	1	34.78	0.4770	0.5004	
X_3	12259.69	1	12259.69	168.13	< 0.0001	
X_4	3266.74	1	3266.74	44.80	< 0.0001	
X_1X_2	81.23	1	81.23	1.11	0.3079	
X_1X_3	91.44	1	91.44	1.25	0.2804	
X_1X_4	5.84	1	5.84	0.0802	0.7810	
X_2X_3	24.33	1	24.33	0.3337	0.5721	
X_2X_4	70.94	1	70.94	0.9729	0.3396	
X_3X_4	653.19	1	653.19	8.96	0.0091	
X_1^2	59.28	1	59.28	0.8130	0.3815	
X_2^2	58.54	1	58.54	0.8029	0.3844	
X_3^2	131.47	1	131.47	1.80	0.1993	
X_4^2	10.91	1	10.91	0.1496	0.7044	
Residual	1093.75	15	79.92			
Lack of Fit	988.68	10	98.87	4.70	0.0506	Not significant
Pure Error	105.07	5	21.01			
Cor Total	19254.16	29				
	Fit Statistics					
Standard Deviation (Std. Dev) = 8.54				R^2 = 0.9432		
Mean = 40.96				Adjusted R^2 = 0.8902		
Coefficient of variation (C.V.) % = 20.85				Predicted R^2 = 0.6591		
				Adeq Precision = 15.6266		

Table 4. ANOVA for the reduced quadratic model of degradation efficiency

Source	Sum of Square	dF	Mean Square	F-value	p-value	
Model	17671.55	5	3534.31	53.60	< 0.0001	Significant
X_1	361.63	1	361.63	5.48	0.0278	
X_3	12259.69	1	12259.69	185.92	< 0.0001	
X_4	3266.74	1	3266.74	49.54	< 0.0001	
X_3X_4	653.19	1	653.19	9.91	0.0044	
X_3^2	1310.31	1	1310.31	17.14	0.0004	
Residual	1582.61	24	65.94			
Lack of Fit	1477.54	19	77.77	3.70	0.0762	Not significant
Pure Error	105.07	5	21.01			
Cor Total	19254.16	29				
	Fit Statistics					
Standard Deviation (Std. Dev) = 8.12				R^2 = 0.9178		
Mean = 40.96				Adjusted R^2 = 0.9007		
Coefficient of variation (C.V.) % = 19.82				Predicted R^2 = 0.8661		
				Adeq Precision = 24.2603		

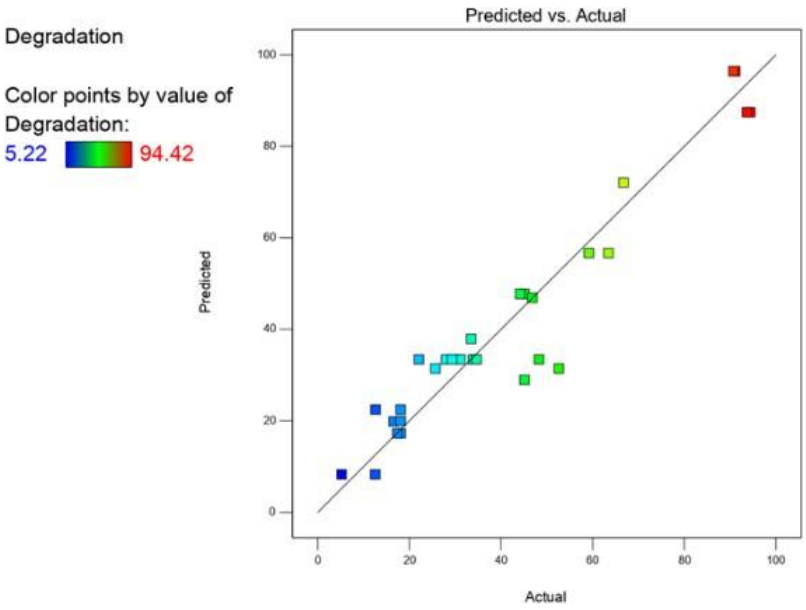

Figure 1. Linear correlation between predicted vs actual values for MO degradation

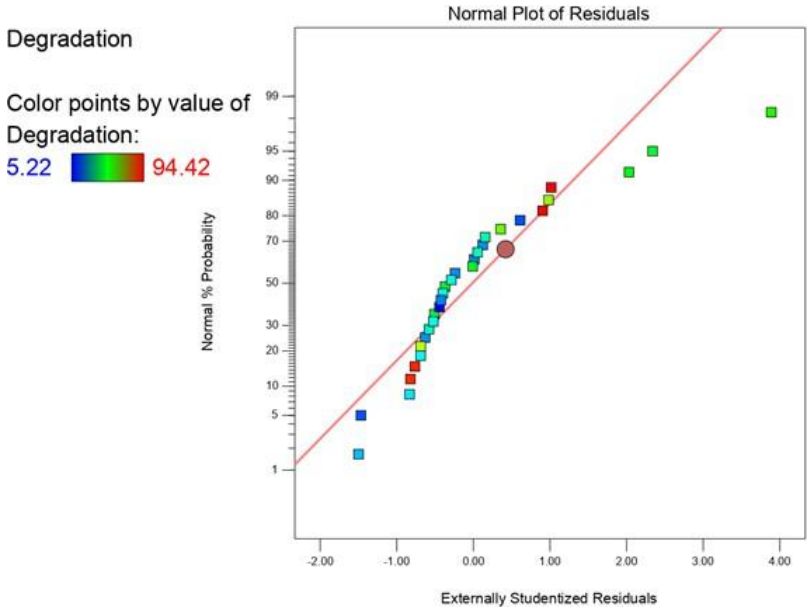

Figure 2. Normal probability plots of residuals

Combined effect of operating parameters on the response

The interactive influence of key variables on the percentage degradation of MO was evaluated using a quadratic response-surface model. Three-dimensional (3D) surfaces and their corresponding two-dimensional (2D) contour plots were generated to visualize how simultaneous changes in two factors affected the response, while the remaining variables were held at their center levels.

The combined effect of pH and catalyst ratio is illustrated in **Figures 3(a)** and **3(b)**. The plots clearly showed that degradation efficiency decreased as the solution pH increased from 9.5 to 11, even at high catalyst loading. This observation aligned with the known reactivity of Fe(III)TAML catalysts, which were designed to function effectively under mild alkaline conditions but could lose activity in strongly basic solutions [13,14]. Chahbane et al. reported that the decomposition of H_2O_2 by Fe (III)TAML becomes non-productive at

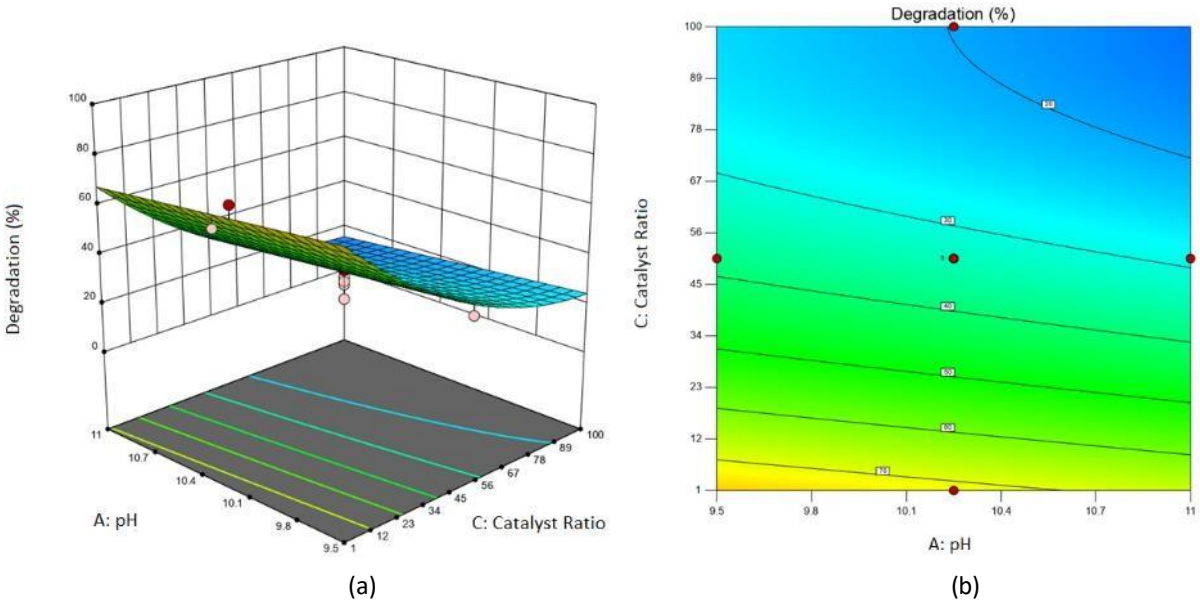

Figure 3. 3D surface (a), and contour (b) plots for combined factors of pH and catalyst ratio on MO degradation

high pH, leading to the preferential formation of O_2 and H_2O_2 instead of the high-valent iron–oxo species (Fe(IV)/Fe(V) = O) responsible for oxidative dye degradation [13]. The horizontal nature of the contour line in **Figure 3(b)** confirmed that pH exerted a stronger influence than the catalyst ratio in this interaction. The highest degradation values (>80%) were achieved at the lower end of the tested pH range (≈9.5-10.0) with a high catalyst ratio, suggesting that the catalytic cycle or generating active oxidants was most efficient in this region [11].

Figures 4(a) and **4(b)** depict the interaction between the catalyst ratio and the dye ratio. Contrary to the intuitive expectation that more catalysts would always lead to better degradation, the model indicated that the degradation percentage decreased as the catalyst ratio increased, while it increased with a higher dye ratio. This counterintuitive trend had been noted in other catalytic oxidation studies [10,12]. A possible explanation is that at high catalyst concentrations, rapid, non-productive decomposition of H_2O_2 occurs, in which oxidant molecules are consumed before they can effectively interact with the target dye molecules [5,15]. This is sometimes referred to as "scavenging" of the reactive species by the catalyst itself or by side reactions. Conversely, a higher initial dye ratio provided more substrate molecules, potentially increasing the probability of collision between the dye and the short-lived ROS, thereby improving the apparent degradation efficiency within the tested range [18]. The significant interaction term (X_3X_4) and the quadratic effect of the catalyst ratio (X_3^2) in the ANOVA (**Table 4**) statistically supported this complex, non-linear relationship, indicating that the effect of catalyst loading was not independent of the pollutant concentration.

Although stirring speed (X_2) was not identified as a statistically significant factor within the investigated range, it played a vital physical role in dye degradation by enhancing mixing, mass transfer, and contact between reactive species. Previous studies have reported that stirring speed can influence MO degradation efficiency depending on the treatment process and operating conditions [19,20]. In the present study, the insignificant effect suggested that adequate mixing was achieved across the selected stirring speed range, and other factors, such as pH, catalyst ratio, and dye ratio, were more dominant in controlling the degradation process.

Numerical analysis and model validation

Numerical analysis using Design-Expert was conducted to identify model-predicted conditions associated with high degradation efficiency within the investigated experimental range, while keeping all factors within the tested ranges. Under these conditions, the model predicted a MO degradation of 96.43 at pH 9.5, stirring speed 500 rpm, catalyst ratio of 1, and dye ratio of 100. To validate the developed model, an experiment was performed under these

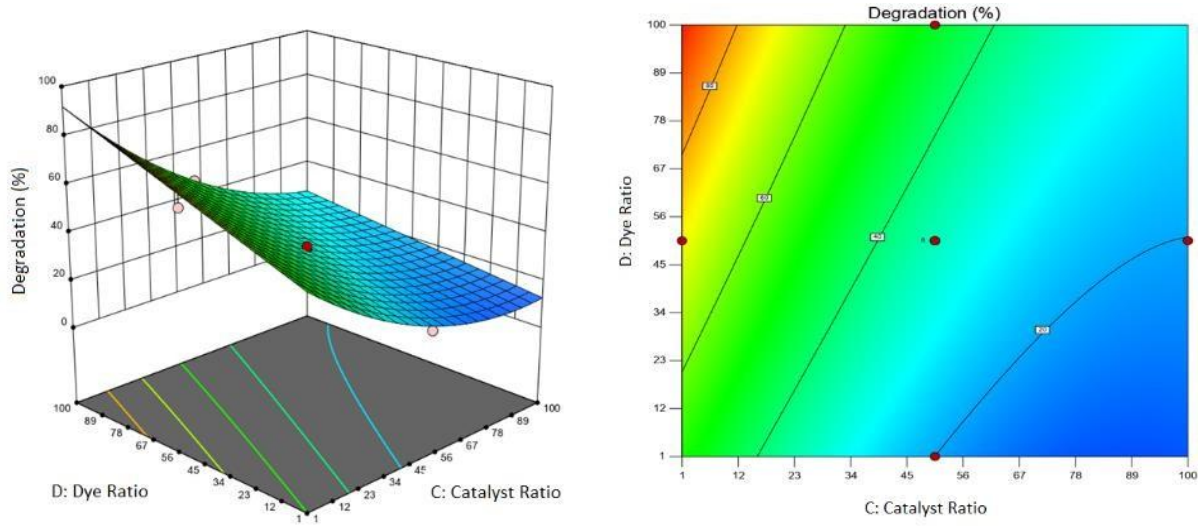

(a) (b)

Figure 4. 3D surface (a), and contour (b) plots for combined factors of catalyst ratio and dye ratio on MO degradation

Table 5. Results of validation experiments

Parameter	pH	Stirring Speed (rpm)	Catalyst Ratio	Dye Ratio	Predicted Degradation (%)	Experimental Degradation (%)	Percentage Error (%)
Optimum	9.5	500	1	100	96.43	92.33	4.25

conditions, yielding an observed degradation of 92.33 %. The percentage error between the predicted and experimental values was 4.25%, indicating excellent agreement between the model and the actual process. This low deviation confirmed the robustness and reliability of the developed RSM model.

The predicted and experimental results are summarized in **Table 5**, which clearly shows the close match between the model prediction and the validation experiment. In addition to performance validation, the sustainability of the catalytic system is an important consideration for practical application. Although reusability studies were not conducted in this work due to the homogenous nature of the Fe(III)TAML catalyst, the time-dependent decrease in MO absorbance during the reaction indicated sustained catalytic activity throughout a single degradation cycle. The experimental design focused on kinetic monitoring rather than catalyst recovery and reuse, which would require separation or immobilization strategies not explored in this study. Nevertheless, catalyst reusability remained a critical factor for long-term sustainability, and future work should focus on developing recovery or immobilization approaches to enable multi-cycle reuse of the Fe(III)TAML-based catalytic systems.

Conclusion

This study confirmed the high efficiency of the Fe(III)TAML/H_2O_2 catalytic system for degrading MO and elucidated the influence and interactions of key operating parameters using RSM. CCD revealed that pH, catalyst ratio, and dye ratio interact significantly to control the degradation rate. Three-dimensional surface and contour analyses showed that lower pH within the tested range and higher dye ratio promoted degradation, whereas excessive catalyst loading reduced it. Numerical analysis based on the developed RSM model predicts 96.43% degradation at pH 9.5, a stirring speed of 500 rpm, a catalyst ratio of 1, and a dye ratio of 100. A validation experiment under these conditions achieved 92.33 % degradation, corresponding to a percentage error of 4.25%, thereby supporting the reliability of the quadratic model. These findings provide a practical operating window for applying the Fe(III)TAML/H_2O_2 system to real wastewater containing azo dyes. Operating near pH 9.5 with a modest catalyst dosage and adequate mixing offers an effective balance between oxidant generation and reagent economy, enabling high-level MO removal

while minimizing chemical and energy inputs. The results highlight the potential applicability of this homogeneous catalytic process for treating dye-contaminated wastewater, and further studies on detailed optimization, scale-up, and long-term performance are recommended to support practical implementation.

Overall, this study demonstrates that the Fe(III)–TAML/H_2O_2 catalytic system is an effective and promising AOP for the degradation of MO, achieving high removal efficiency under optimized conditions determined by RSM. The findings contribute to a better understanding of environmentally friendly catalytic systems for dye-contaminated wastewater and highlight the potential of Fe(III)–TAML catalysts as viable alternatives to conventional treatment methods. This work provides a scientific foundation for the development of efficient, sustainable, and scalable wastewater treatment strategies to mitigate the environmental impacts of persistent dye pollutants.

Acknowledgement
This research was financially supported by the Universiti Malaysia Terengganu (UMT) through the Talent and Publication Enhancement Research Grant (UMT/TAPE-RG/2020/55278)

References

1. Lin, L., Yang, H., and Xu, X. (2022). Effects of water pollution on human health and disease heterogeneity: A review. *Frontiers in environmental science*, 10: 880246.
2. Liu, Q. (2020). Pollution and treatment of dye Waste-Water. *IOP Conference Series Earth and Environmental Science*, 514(5): 052001.
3. Liu, Y., Chen, J., Duan, D., Zhang, Z., Liu, C., Cai, W., and Zhao, Z. (2024). Environmental impacts and biological technologies toward sustainable treatment of textile dyeing wastewater: A review. *Sustainability*, 16 (24): 2071-1050.
4. Science History Institute. William Henry Perkin. Access from https://www.sciencehistory.org/education/scientific-biographies/william-henry-perkin/ [Access online 2 August 2025]
5. Katheresan, V., Kansedo, J., and Lau, S. Y. (2018). Efficiency of various recent wastewater dye removal methods: A review. *Journal of Environmental Chemical Engineering*, 6 (4): 4676-4697.
6. Iwuozor, K. O., Ighalo, J. O., Emenike, E. C., Ogunfowora, L. A., and Igwegbe, C. A. (2021). Adsorption of methyl orange: A review on adsorbent performance. *Current Research in Green and Sustainable Chemistry*, 4: 100179.
7. Hashemi, S. H., and Kaykhaii, M. (2022). Emerging freshwater pollutants ebook. Elsevier, Netherland: pp. 267–287.
8. Khan, A. U., Zahoor, M., Rehman, M. U., Shah, A. B., Zekker, I., Khan, F. A., Ullah, R., Albadrani, G. M., Bayram, R., and Mohamed, H. R. H. (2022). Biological Mineralization of Methyl Orange by Pseudomonas aeruginosa. *Water*, 14(10): 1551.
9. Santos, S. C. R., and Boaventura, R. A. R. (2019). Treatment of azo dyes in industrial effluents: A review on biological versus physical-chemical treatments. *Journal of Environmental Chemical Engineering*, 7(5): 103309.
10. Demirel, M., and Kayan, B. (2012). Application of response surface methodology and central composite design for the optimization of textile dye degradation by wet air oxidation. *International Journal of Industrial Chemistry*, 3: 1-10.
11. Ghosh, P., Das, R., and Ghosh, M. (2020). Oxidative degradation of azo dyes using Fe(III)TAML/H_2O_2: A comprehensive review of process kinetics and mechanisms. *Journal of Environmental Management*, 261: 110229.
12. Wang, H., Liu, Z.-H., Zhang, J., Huang, R.-P., Yin, H., Dang, Z., Wu, P.-X., and Liu, Y. (2019). Insights into removal mechanisms of bisphenol A and its analogues in municipal wastewater treatment plants. *The Science of the Total Environment*, 692: 107–116.
13. Naima Chahbane, Popescu, D.-L., Mitchell, D. A., Chanda, A., Lenoir, D., Ryabov, A. D., Schramm, K.-W., and Collins, T. J. (2007). Fe(III)–TAML-catalyzed green oxidative degradation of the azo dye Orange II by H2O2and organic peroxides: products, toxicity, kinetics, and mechanisms. *Green Chemistry,* 9(1): 49–57.
14. Espinoza-Montero, P. J., Burneo, C., Cevallos, A., G. Xavier Castillo-Cabrera, Sofía Peñafiel-Vicuña, Martínez-Huitle, C., Lenys Fernández, and Mora, J. R. (2023). Application of an Fe-TAML/H_2O_2 system for rapid degradation of organic matter. *Journal of Environmental Chemical Engineering,* 11(5): 110994–110994.
15. Xian, Z., Liang, S., Jin, X., Tian, H., Ling, J., and Wang, C. (2020). Application of Fe(III)-TAML/H_2O_2 system for treatment of fluoroquinolone antibiotics. *Journal of Environmental Sciences*, 99: 110–118.
16. Montgomery, D. C. (2017). Design and analysis of experiments (9th edition). Wiley.
17. Ohale, P., Uzoh, C., and Onukwuli, O. (2017).

Optimal factor evaluation for the dissolution of alumina from Azaraegbelu clay in acid solution using RSM and ANN comparative analysis. *South African Journal of Chemical Engineering*, 24: 43–54.

18. Xu, H.-Y., Shi, T.-N., Zhao, H., Jin, L.-G., Wang, F.-C., Wang, C.-Y., and Qi, S.-Y. (2015). Heterogeneous Fenton-like discoloration of methyl orange using Fe_3O_4/MWCNTs as catalyst: process optimization by response surface methodology. *Frontiers of Materials Science*, 10(1): 45–55.
19. Feng, Q., Tang, Y., Wang, K., Wu, C., and Huang, X. (2025). Study on the degradation of methyl orange by UV-acetylacetone advanced oxidation system. *Desalination and Water Treatment*, 321: 100928.
20. Sunil R., Anjali G., Garvita G., Bhawana C., Girish T., Singh P.A., Kumar J.A.(2020) Fenton oxidation process for the treatment of artificial binary dye mixture in aqueous solution. *Research Journal of Chemistry and Environment*, 24 (7): 70 – 80.
21. Bawazeer, S. (2024). A potential eco-friendly degradation of methyl orange by water-ball (sodium polyacrylate) stabilized zero valent iron nanoparticles. *Heliyon,* 11(1): e41226.
22. Xu, H.-Y., Shi, T.-N., Zhao, H., Jin, L.-G., Wang, F.-C., Wang, C.-Y., and Qi, S.-Y. (2015). Heterogeneous Fenton-like discoloration of methyl orange using Fe_3O_4/MWCNTs as catalyst: process optimization by response surface methodology. *Frontiers of Materials Science*, 10(1): 45–55.
23. Abibu, W. A., Bamigbade, G., Kolawole, A. O., Ajayi, T., and Sakariyau, A. W. (2021). Current trends in steroidal 17α-ethynylestradiol (EE2) removal from the environment: A review. *Applied Environmental Research*, 43(2): 130-158.
24. Abu Hasan, H., Muhamad, M. H., Budi Kurniawan, S., Buhari, J., and Husain Abuzeyad, O. (2023). Managing bisphenol A contamination: advances in removal technologies and future prospects. *Water*, 15 (20): 3573.
25. Acikses, A., Taskan, G., and Barim, G. (2018). A study on copolymer systems of styrene with diethanolamine side group and methyl methacrylate. *Journal of Chemistry*, 2018(1): 8957267.
26. Aerni, P. (2004). Risk, regulation and innovation: The case of aquaculture and transgenic fish. *Aquatic sciences*, 66: 327-341.
27. Aghili, F., Ghoreyshi, A. A., Rahimpour, A., and Rahimnejad, M. (2017). Coating of mixed-matrix membranes with powdered activated carbon for fouling control and treatment of dairy effluent. *Process Safety and Environmental Protection*, 107: 528-539.
28. Amini, M., Younesi, H., Bahramifar, N., Lorestani, A. A. Z., Ghorbani, F., Daneshi, A., and Sharifzadeh, M. (2008). Application of response surface methodology for optimization of lead biosorption in an aqueous solution by *Aspergillus niger*. *Journal of hazardous materials*, 154 (1-3): 694-702.
29. Anan, N. S. M., Jaafar, J., Othman, M. H. D., Rahman, M. A., Aziz, F., and Shahrodin, N. S. M. (2019). Titanium dioxide incorporated thin film composite membrane for bisphenol A removal. *Malaysian Journal of Fundamental and Applied Sciences*, 15 (5): 755-760.
30. Bhatnagar, A., and Anastopoulos, I. (2017). Adsorptive removal of bisphenol A (BPA) from aqueous solution: A review. *Chemosphere*, 168: 885-902.
31. Box GEP, Draper NR (1978) Empirical model-building and response surfaces. Wiley, New York
32. Cao, Z., Yang, C., Zhang, W., and Shao, H. (2024). Activated persulfate for efficient bisphenol A degradation via nitrogen-doped Fe/Mn bimetallic biochar. *Water Science & Technology*, 90(4): 1149-1163.
33. Chen, Y., Shi, Y., Wan, D., Liu, Y., Wang, Y., Han, X., and Liu, M. (2022). Degradation of bisphenol A by iron-carbon composites derived from spent bleaching earth. *Colloids and Surfaces A: Physicochemical and Engineering Aspects*, 639: 128376.
34. Hu, Y., Zhu, Q., Yan, X., Liao, C., and Jiang, G. (2019). Occurrence, fate and risk assessment of BPA and its substituents in wastewater treatment plant: A review. *Environmental Research*, 178: 108732.
35. Imane, O., Certin, M., Petit, E., Lesage, G., Abderrahmane, D., Abdallah Ouagued, and Lacour, S. (2025). Screening refractory dye degradation by different advanced oxidation processes. *Molecules*, 30 (3): 712-712.
36. Lim, CL, Morad, N, Teng, TT, and Norli I. (2011) Chemical oxygen demand (COD) reduction of a reactive dye wastewater using H_2O_2/pyridine/Cu(II) system. *Desalination* 278: 26–30
37. Malik, S. N., Ghosh, P. C., Vaidya, A. N., and Mudliar, S. N. (2018). Catalytic ozone pretreatment of complex textile effluent using Fe^{2+} and zero valent iron nanoparticles. *Journal of Hazardous Materials*, 357: 363-375.
38. Mukhopadhyay, A., Sharma, M., and Sharma, K. P. (2020). Dispersion and interaction of charged fluorescent dyes in protein-polymer surfactant-based non-aqueous liquid. *ChemPhysChem*, 21(18): 2127-2135.

39. Nath, A., Biswas, S., and Pal, A. (2022). A comprehensive review on BPA degradation by heterogeneous Fenton-like processes. *Water Science & Technology*, 86(4): 714-745.
40. Ohore, O. E., and Zhang, S. (2019). Endocrine disrupting effects of bisphenol A exposure and recent advances on its removal by water treatment systems. A review. *Scientific African*, 5: e00135.
41. Sharma, K., Yadav, A., and Jain, R. (2021). Fe(III)TAML/H_2O_2 as a catalyst system for the removal of textile dyes: Kinetics and environmental benefits. *Environmental Progress & Sustainable Energy*, 40(2): e13487.
42. Yatim, H. M., Aruldass, C. A., Hamzah, M. A. A. M., Ahmad, W. A., and Setu, S. A. (2019). Synthesis and optimization of nano-sized bacterial-based violacein pigment using response surface methodology. *Malaysian Journal Fundamental Applied*, 15: 818-24.
43. Zhang Z, Zheng H (2009) Optimization for decolorization of azo dye acid green 20 by ultrasound and H2O2 using response surface methodology. *Journal Hazardous Materials*, 172: 1388–1393
44. Zhang, W., Fang, Y., Shi, X., Zhang, M., Wang, X., and Tan, Y. (2012). Effect of bisphenol A on the EGFR- STAT3 pathway in MCF-7 breast cancer cells. *Molecular Medicine Reports*, 5(1): 41-47.